Marine Systems & Ocean Technology (2020) 15:26–44
https://doi.org/10.1007/s40868-020-00072-6

ORIGINAL PAPER

An exergy analysis of various layouts of ORC-VCC systems for usage in waste heat recovery onboard ships

Oumayma Bounefour[1] · Ahmed Ouadha[1] · Yacine Addad[1,2]

Received: 6 February 2019 / Accepted: 10 February 2020 / Published online: 19 February 2020

Abstract
An exergy based analysis is carried out for waste heat recovery from a marine Diesel engine using various layouts of organic Rankine cycles (ORCs) for driving a vapor compression refrigeration cycle. The ORC layouts studied are a simple organic Rankine cycle (ORC), an organic Rankine cycle with internal heat exchanger (RORC) and a serial cascade ORC cycle (SCORC). In addition to the well-known fluid R134a, two hydrocarbon-based refrigerants, namely butane (R600) and isobutane (R600a), are considered in the present study. It is found that sensible improvements are attained using the cascade ORC and the ORC with internal heat exchanger configurations compared to simple ORC under certain conditions. This improvement depends on both the heat source temperature and the working fluid considered. Moreover, the results indicate that R600 as working fluid has the best performance from a thermodynamic point of view. Finally, though R600, a pure hydrocarbon, is completely accepted by the environment, more attention should be paid to its flammability.

Abbreviations

COP	Coefficient of performance
CPR	Compressor pressure ratio
EVR	Expander volume ratio
Ex	Specific exergy, kJ/kg
$\dot{E}x$	Exergy rate, kW
H	Specific enthalpy, kJ/kg
M	Molecular weight, kg/kmol
$\dot{m}$	Mass flow rate, kg/s
P	Pressure, MPa
T	Temperature, K
V	Specific volume, m^3/kg
$\dot{Q}$	Heat transfer rate, kW
$\dot{W}$	Power rate, kW

Greek symbols

$\Delta\dot{E}x$	Exergy loss rate, kW
η	Efficiency

Subscripts

b	Boiler
Exp	Expander
evap	Evaporator/evaporation
cond	Condenser/condensation
comp	Compressor
ORC	Organic Rankine cycle
VCC	Vapor compression cycle
Tot	Total
Sat	Saturation/saturated
L	Liquid
P	Constant pressure/pump
S	Specific entropy, kJ/kg K

Exponents

°	Ideal gas state

1 Introduction

Looked at as the most reliable and cost-effective mean of transportation, shipping has become the backbone of the world's economy. In fact, more than 80% of the world's trade is achieved by sea-going vessels [1] unfortunately leading to huge amount of pollutants emissions. The majority of today sea-going vessels are propelled using Diesel engines.

✉ Ahmed Ouadha
ah_ouadha@yahoo.fr

Yacine Addad
ah_ouadha@yahoo.fr

[1] Laboratoire, Sciences Et Ingénierie Maritimes, Faculté de Génie Mécanique, Université Des Sciences Et de La Technologie Mohamed BOUDIAF D'Oran, Oran El-Mnouar, 31000 Oran, Algérie

[2] Department of Nuclear Engineering, Khalifa University of Science and Technology (KUST), PO Box 127788, Abu Dhabi, UAE

This kind of propulsion systems allows a superior efficiency with the possibility of burning heavy fuel oil. Although their emissions are still marginal compared to the ones emitted from land vessels and air transport (IMO, 2014), their growing trend is worrying [2].

During its operation, a ship produces various types of solid, liquid and gaseous wastes such as; rubbish, sludge, ballast, water and air emissions. The latter is produced during the combustion of fossil fuels but has been for longtime ignored by legislation as its quantity is lower compared to the emissions produced by the air and land vessels. Indeed, CO_2 emissions caused by shipping represent only 2–4% of the global emissions [3]. Unfortunately, the ratio of shipping related CO_2 emissions is expected to increase up to 12–18% by 2050 according to the study carried out by [4]. The 2018 International Maritime Organization (IMO) targets for low- and zero-emission shipping aspire to reduce the total annual greenhouse gases (GHGs) emissions by at least 50% by 2050 over 2008 levels and phase them out, as soon as possible in this century.

Furthermore, it is also estimated that shipping related NOx emissions are responsible for 15% of global NOx emissions [5]. Due to their harmful effects on human health and environment, the NOx emissions have been subject to stringent regulations formulated in the MARPOL Annex 6 by the IMO.

Facing these increasingly environmental policies, shipbuilders must develop energy-saving technologies for all types of ships. Det Norske Veritas (DNV) proposed several operational and design measures such as weather routing, hydrodynamic form optimization and engine refinements that should potentially reduce CO_2 emissions from the new designs and existing fleet [6]. Among these measures, the treatment of waste heat onboard of ships is a very promising way to save energy and reduce pollutant emissions. Interestingly, waste heat from the ship propulsion systems can reach up to 210 MWh per year. Consequently, several proposals have been put forward to recover heat onboard of ships. Amongst these technologies one can cite; steam production [7], ballast water treatment [8], freshwater production [9] and cooling and cogeneration [10, 11]. However, it is worth mentioning here that a large proportion of this heat remains unrecoverable since its temperature is relatively low. Actually, the low-temperature waste heat (lower than 150 °C) recovery has been for decades ignored due to the associated high investment costs. Nevertheless, energy saving can be achieved by promoting the utilization of this low-temperature waste heat such as engine jacket cooling water and Organic Rankine Cycle (ORC) technologies should be able to meet this ambition. An ORC is in essence a Rankine cycle, but it is using an organic fluid as the working fluid instead of water. This type of cycles has been widely used to produce power from solar and geothermal heat sources [12, 13] and has been only recently considered to recover the waste heat from marine Diesel engines [14–16].

The onboard ship-refrigeration systems are heavily demanding in terms of fuel consumption. In fact, [17] estimated that 25% of total gaseous emissions are associated to the whole operation of heating, ventilation and air-conditioning (HVAC) and refrigeration systems on board. This is due to the fact that this kind of systems requires additional fuel consumption to produce the mechanical power required to drive their compressors. Thus, potential energy savings can be achieved by using the waste heat on board of the ships to drive these HVAC and refrigeration systems.

Basically, two approaches can be used to recover waste heat from a marine Diesel engine to produce cooling effect. The first one utilizes waste heat as a heat source for driving directly a refrigeration system (ejector, absorption or adsorption refrigeration systems), and the second one converts the waste heat into mechanical or electrical power to drive a vapor compression refrigeration system. The reader can refer to a recent review paper by [18] on the progress and prospect of utilizing different kinds of heat driven fishing vessel refrigeration systems, i.e., adsorption refrigeration system, absorption refrigeration system, ejection refrigeration system and hybrid systems, with a special focus on the techniques for improving system efficiency and its operational stability under severe conditions on seas. In particular, the idea of using an organic Rankine cycle as a heat recovery system which can then drive a vapor compression cycle (known as combined ORC-VCC system) should be able to satisfy refrigeration and air-conditioning requirements and might even produce additional power when cooling is not required onboard.

The concept of ORC-VCC systems is not new. First studies on ORC-VCC systems have been carried out more than 40 years ago [19, 20]. It was considered by several researchers as a promising solar cooling method [21–26]. The abandonment of ORC-VCC during a decade as justified by the hollow of literature from 1994 to 2004, as illustrated in Table 1, may be attributed to the halocarbon compounds (R113, R114), which have been considered among the best candidates for ORC subsystems. Environmental and energy savings issues have increased the interest in ORC-VCC systems using different low-grade heat sources such as solar energy, geothermal energy and internal combustion engines exhaust gases. The development of HFC refrigerants (R134a, R245fa) has marked a renewed interest in ORC-VCC systems during the 2000s. Thus, as illustrated in Table 2, great efforts have been devoted to the development of the ORC-VCC technology. Table 2 summarizes experimental and theoretical studies carried on ORC-VCC systems since their first adoption in the 1970s.

With regards to synthetic refrigerants, R134a and R410a are widely used in refrigeration and air-conditioning

Table 1 Previous studies on ORC-VCC systems

Year	Authors	Study	Working fluids	Heat source	Remarks
1975	Prigmore and Barber [19]	Exp	R12, R113	Solar energy	Maximum COP = 0.5
1977	Lior [20]	Theo	Water steam (ORC)	Solar energy	50–60% Energy savings
1980	Wali [21]	Exp	R11, R113, R114, FC75, FC88	Solar energy	FC88 and R113 are leading candidates fluids
1982	Biancardi et al. [22]	Exp	R11, R113, R113A, R114	Solar energy	R11 $COP_{heating}$ = 1.6–2.25 R11 $COP_{cooling}$ = 0.5–0.75
1982	Nazer and Zubair [23]	Theo	R22, R114	Low-grade heat	Use of separate condensers
1984	Koai et al. [24]	Exp	Water steam (ORC)	Solar energy	20–26% from non-solar sources double the efficiency of solar ORC
1986	Egrican and Karakas [25]	Theo	R22, R114	Solar energy	Boiler produces the greatest exergy destruction
1990	Christensen and Santoso [26]	Theo	R22, R113	Fossil fuel burning	$COP_{heating}$ = 2.01 $COP_{cooling}$ = 1.06
1994	Kaushik et al. [45]	Theo	R12, R113, R114, R22	Low-grade heat Solar energy	Rl14 + R22 and Rl13 + R22 showed the best performance
2004	Jeong and Kang [46]	Theo	R123, R134a, R245ca	Natural gas burning	R245fa is the best candidate
2010	Aphornratana and Sriveerakal [47]	Theo	R22, R134a	Low-grade heat	R22 provided better COP than R134a
2011	Wang et al. [48]	Exp	R245fa	Low-grade heat	COP = 0.5
2011	Wang et al. [49]	Theo	R245fa	Low-grade heat	Subcooling and recuperation in the VCC gave COP = 0.66
2011	Little and Garimella [41]	Theo	R245fa	Low-grade heat	$COP_{AR} > COP_{ORC-VCC}$
2012	Aneke et al. [50]	Theo	R245fa, NH_3	Low-grade heat	$COP_{ORC-VCC} > COP_{AR}$
2012	Demierre et al. [51]	Exp	R134a	Methane burning	–
2013	Li et al. [52]	Theo	R290, R600, R600a, R1270	Solar energy Geothermalenergy	R600 performed the best
2013	Bu et al. [53]	Theo	R123, R134a, R245fa, R600a, R600	Geothermal energy	R600a performed the best
2013	Bu et al. [54]	Theo	R123, R245fa, R600, R600a, R600, R290	Solar energy	R123 performed the best
2014	Bu et al. [55]	Theo	R123, R134a, R245fa, R600, R600a, R600, R290	Waste heat from a marine Diesel engine	R600a performed the best
2014	Demierre et al. [56]	Exp	R134a	Methane burning	–
2014	Li et al. [57]	Theo	R22, R134a, R290	Low-grade heat	R134a performed the best
2014	Bounefour and Ouadha [27]	Theo	R134a, R290, R600, R600a, R1270	Waste heat from a marine Diesel engine	R600 and R600a yielded the highest performance
2015	Yilmaz [58]	Theo	R134a, R245fa	Bus engine exhaust gas	Both refrigerants were recommended for this application
2015	Molés et al. [59]	Theo	R245fa, R1233zd(E), R1336mzz(Z)	Low-grade heat	R1234ze (E)-VCC/R1336mzz (Z)- ORC performed the best
2015	Kim and Blanco [60]	Theo	R143a, R22, R134a, R152a, R290, R717, R600, R600a	Low-grade heat	working fluids with higher critical temperature provided higher thermal efficiency
2016	Yue et al. [61]	Theo	n-propane, cyclopentane, R134a, R245fa	Engine exhaust gases	R134a performed the best
2016	Nasir and Kim [62]	Theo	R245fa, R123, R134a, R1234yf, R1234ze (E), R600, R600a, R245fa, R123	Low-grade heat	R134a-ORC/R600a-VCC was the best combination

Table 1 (continued)

Year	Authors	Study	Working fluids	Heat source	Remarks
2016	Karellas and Braimakis [63]	Theo	R134a, R152a, R245fa	Biomass fuel Solar energy	R245fa performed the best
2016	Saleh [64]	Theo	1270, R290, RC318, R236fa, R600a, R236ea, R600, R245fa, R1234ze(E), R1234yf	Low-grade heat	R600 performed the best
2017	Lizarte et al. [65]	Theo	Toluene, NH_3/CO_2	Low-grade heat	Maximum COP = 0.79
2017	Wu et al. [66]	Theo	R134a	Solar energy	The system was twice more expensive than a conventional cooling system
2017	Braimakis et al. [67]	Theo	R245fa, hexane, cyclohexane	Biomass fuel Solar energy	R245fa for ORC-VCC was the most cost-effective scenario
2017	Bounefour and Ouadha [68]	Theo	R134a, R290, R600, R600a, R1270	Waste heat from a marine Diesel engine	R600 and R600a yielded the highest performance
2018	Saleh [69]	Theo	R600, R600a, R601, R601a, R602, RC318, C5F12, R152a, R236ea, R236fa, R245ca, R245fa, RE245cb2, R1234ze(E)	Low-grade heat	R602 performed the best
2018	Zheng et al. [70]	Theo	R290, R161, R152a, R134a, R600a, R227ea, R1234yf, R1234ze, R290/R600a, R152a/R600a, R161/R600a, R227ea/R600a, R1234yf/R600a	Solar energy	R161/R600a with an R161 mass fraction of 0.25 showed the highest system efficiency (0.3089)
2019	Javanshir et al. [71]	Theo	R134a, R22, R143a	Geothermal energy	R22 and R143a exhibited the highest energy and exergy efficiencies, respectively
2019	Saleh et al. [72]	Theo	R161, RC318, R600, R601, R600a, R601a, R152a, R602, Perfluoropentane, R245ca, R236fa, R245fa, R236ea, RE245cb2, R602a,R1234ze(E), RE245fa2, RE170, RE347mcc, R365mfc,R603, R604, Cyclopentane	Renewable energy	Cyclopentane accomplished the highest system performance
2019	Nasir et al. [73]	Theo	R245fa, R600, R600a, R134a	Low-grade heat	R600a ORC-R245fa VCC was the option
2019	Liang et al. [74]	Theo	R134a, R1233zd, R1234zez, R245fa, R245ca	Engine exhaust gases	R245ca-ORC/R134a-VCC accomplished the best performance

Table 2 Refrigerant properties [40]

Refrigerant	Molecular mass (g/mol)	Boiling point (°C)	Critical temperature (°C)	Critical pressure (MPa)	Safety group	GWP
R134a	102.03	− 26.1	101.1	4.06	A1	1430
R600	58.12	− 0.5	152.0	3.80	A3	20
R600a	58.12	− 11.7	134.7	3.63	A3	20

systems but have been recognized as harmful gases. Their global warming potential (GWP) is very high and are considered as strong global warming gases. On the contrary, hydrocarbons such as propane (R290), isobutane (R600a) and propylene (R1270) are environmental friendly natural working fluids having zero ozone depleting potential (ODP) and negligible global warming potential (GWP < 20). This is in addition to their excellent thermodynamic properties, their low price and abundance in nature.

Hence the aim of the present study is to build on the previous preliminary conclusions reported by [27]. In that study, several working fluids including propane, butane, isobutane and propylene have been used to analyze the feasibility of using waste heat from marine Diesel engines to drive a vapor compression refrigeration system. In that paper the authors have successfully demonstrated, through a thermodynamic analysis, that isobutane (R600a) and butane (R600) yield the highest performance, whereas propane (R290) and propylene (R1270) yield negligible improvement compared to R134a for the operating conditions considered [27]. However, as the combined ORC-VCC technique is expected to require high investment cost, a thermodynamic analysis of different ORC-VCC layouts for marine engines waste heat recovery, using friendly refrigerants, is deemed essential in order to promote the application of this technology onboard ships and estimate the theoretical gain of power and energy savings. To achieve this ultimate goal, a comparative study of various configurations of a combined ORC-VCC system is conducted in the present study. The combined system proposed here is composed of an ORC subsystem and a VCC subsystem. I.e., the mechanical power produced by the ORC subsystem is used to drive the VCC subsystem. Different design strategies of the ORC subsystems are considered. Using simplified thermodynamic simulations, a basic ORC system is used as a reference to compare two configurations of ORC systems including ORC with internal heat exchanger and serial cascade cycles in terms of power production and cooling effect when used to drive VCC subsystems. In sum, it is a study from a feasibility project done for an Algerian company interested in onboard alternative refrigeration systems.

2 Thermodynamic modeling

2.1 Description of the system

Useful energy can be produced using a basic ORC system composed of a boiler, a turbine, a condenser and a pump. However, the thermal efficiency of such system is very low. This can be improved by changing the configuration of the system adding more components to optimize the system. Basically, two options are available; the first one uses an internal heat exchanger to extract an amount of the superheated working fluid from the turbine to preheat the subcooled working fluid discharged from the pump, while in the second option, an extra boiler is added either in series or parallel to the boiler of the basic system.

Schematics and the corresponding *T*–*s* diagrams of various configurations of ORC systems, including a basic ORC system, ORC with internal heat exchanger system and a cascade ORC system, and a VCC system are presented in Fig. 1. A basic ORC cycle consists of a pump, a condenser, a boiler and an expander (Fig. 1a). The saturated liquid refrigerant is pressurized by the pump (1–2). The compressed liquid enters the boiler where it is heated, vaporized and superheated using the waste heat from the Diesel engine (2–3). The superheated vapors are expanded in the expander to produce mechanical power.

For the RORC cycle, an internal heat exchanger (IHE) is included between the expander exit and the boiler in order to recover additional heat. This is used to preheat the working fluid before it enters the boiler by extracting heat from the high-temperature working fluid leaving the expander (Fig. 1b). The vapor produced in the boiler is sent to the expander which drives the VCC compressor. The expanded vapor is directed to the IHE to heat up the liquid working fluid leaving the pump. Then the vapor is converted back into a liquid in the condenser by releasing heat to a cooling medium. The liquid obtained is fed back to the boiler by the pump to start a new cycle. As a result, the IHE is expected to increase the exergy efficiency of the cycle by reducing the heat transfer temperature difference.

A cascaded organic Rankine cycle (SCORC) is composed of a high-temperature loop (HT) and a

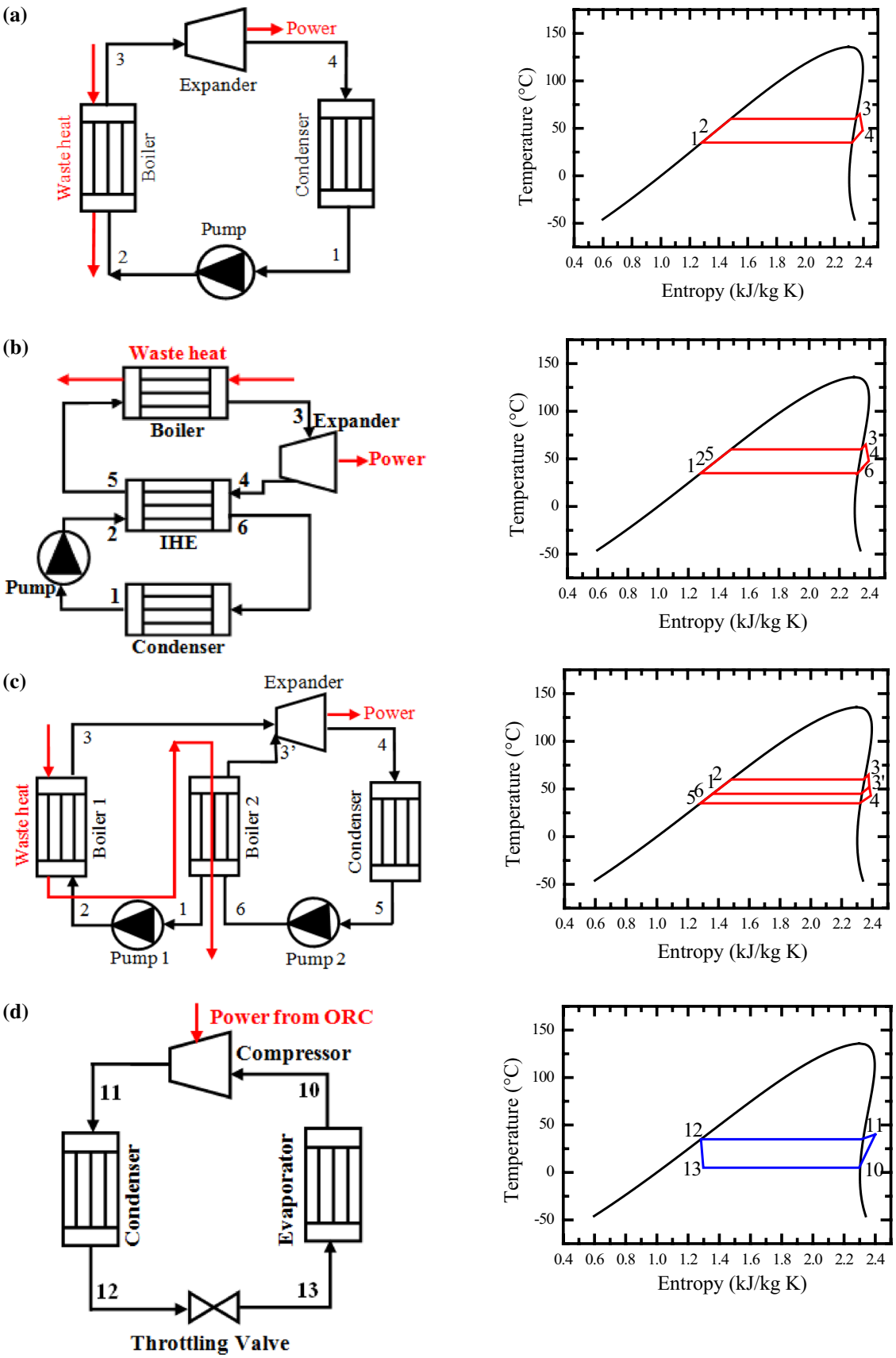

Fig. 1 Schematic and *T-s* diagrams of the selected ORC systems and VCC system: **a** simple ORC; **b** ORC with internal heat exchanger; **c** cascade ORC; **d** VCC

low-temperature loop (LT) (Fig. 1c). It consists of a high-pressure boiler 1, a low-pressure boiler 2, a high-pressure pump 1, a low-pressure pump 2, a turbine and a condenser. The specific liquid working fluid from the condenser is first pressurized to flow into the boiler 2 where it is heated by waste heat from the engine. A portion of the saturated liquid at the saturated pressure in the boiler 2 is pumped to the boiler 1 to be heated by waste heat. The vapor at the state points 3 and 3′ flows into the corresponding stages of the turbine to produce mechanical energy to drive the compressor of the VCC system. The expanded vapor from the turbine is led to the condenser where it is condensed by contact with cold heat source. Finally, the liquid obtained is pumped back by pump 2 to undergo a new cycle.

The power produced by the ORC system is used to drive a vapor compression refrigeration system. The latter consists of a compressor, a condenser, a throttling valve and an evaporator. Vapor from the evaporator is compressed in the compressor. The superheated vapor is then cooled and condensed in the condenser before being throttled to reach the evaporator pressure. During its evaporation, the refrigerant receives heat from the cooling space.

2.2 Working fluids selection

The overall performance of the combined ORC-VCC system depends on the choice of the working fluid used and the configuration of the ORC subsystem. Synthetic refrigerants are commonly proposed to substitute high-GWP HFC-based refrigerants due to their excellent thermodynamic properties with low GWP though their long-term impact on the environment is not known. The ideal solution, according to several researchers [28–38], can be achieved by the reconsidering natural refrigerants. Among these refrigerants, hydrocarbons refrigerants exhibit excellent properties in terms of cooling capacity and efficiency in addition to a low GWP. A refrigeration system designed with given evaporation and condensation temperature would perform comparably for two refrigerants with comparable vapor pressures. As depicted in Fig. 2, the differences of the pressure–temperature curves between R134a and R600 and R600a are small within large interval of temperatures. From a thermodynamic point of view, R600 and R600a can cover greater condensation temperature due to their high critical temperatures with lower pressures. For instance, up to the safety pressure limit of 20 bars, R600 and R600a can operate with a condensation temperature greater than 90 °C.

Hence if used in a good design and with some cautions due to their status as ASHRAE-rated high flammable (A3) refrigerants, hydrocarbons can be energy efficient, environmental friendly and safe to use [39].

Following the preliminary conclusions presented in [27], R600 and R600a are selected as the working fluids for the ORC-VCC systems due to their relatively highest performance in comparison with other hydrocarbons. The properties of these selected fluids are summarized in Table 2 [40].

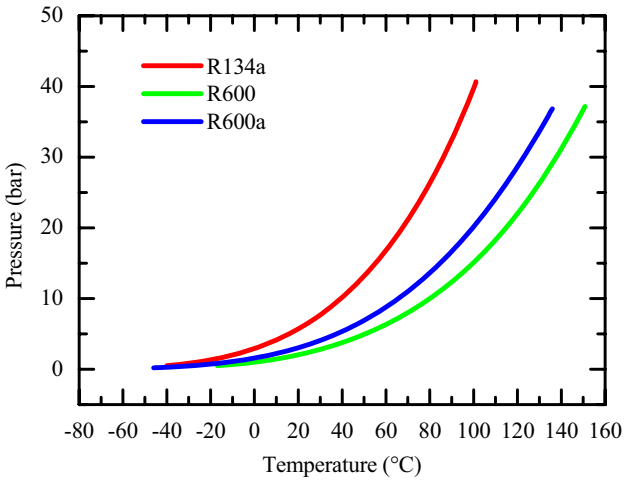

Fig. 2 Vapor pressure vs. temperature curves comparison

It is worth mentioning here that working fluids can be classified as wet, isentropic or dry according to the slope of the saturated vapor curve in an entropy-temperature diagram. That is to say, if the slope is negative, the fluid is classified as wet (e.g.: R134a), while a dry fluid has a positive slope (e.g.: R600, R600a). Finally a fluid is classified as isentropic when its saturated vapor curve has a slope of infinity. Therefore, caution is required when using wet fluids by superheating the vapor at the boiler in order to avoid corrosion.

The analysis of ORC and refrigeration cycles using hydrocarbon-based refrigerants requires an accurate knowledge of their thermodynamic properties. Generally, thermodynamic properties such as enthalpy and entropy of refrigerants are determined using a set of equations of state. The latter are developed based on p–v–T measurements at both the saturation and gaseous states. Four local equation of state including an equation of state of the gas phase, a correlation of the vapor pressure as function of temperature, a correlation of the density of saturated liquid and the ideal gas heat capacity are required. The computational model adopted in this study is based on four local equations of state presented as follows:

– an equation of state for the gas state,

$$Z = Z(T, \rho) \tag{1}$$

– a correlation for the saturated vapor pressure,

$$p_s = p_s(T) \tag{2}$$

– a correlation for the saturated liquid density,

$$\rho_{\mathrm{L}} = \rho_{\mathrm{L}}(T) \tag{3}$$

– an equation of the specific heat capacity at constant pressure in the ideal gas state.

$$c_p^0 = c_p^0(T). \tag{4}$$

Using the above equations and the differential equations of thermodynamics, it is possible to calculate the other essential thermodynamic functions necessary for the thermodynamic analysis, namely, enthalpy, entropy and exergy. Their final expressions have been coded as Fortran Functions to be included in the Fortran code developed for the cycle analysis.

2.3 Thermodynamic analysis

Conventionally, ORC and refrigeration systems are analyzed using the first law of thermodynamics which embodies the energy conservation. However, this method does not consider the quality of energy in the system. For example, it does not recognize any energy losses during a throttling process. On the other hand, exergy analysis, a concept based on the first and second laws of thermodynamics, is a much more powerful metric to evaluate energy systems including ORC, refrigeration and air-conditioning systems. The exergy analysis should be able to provide additional information regarding the system thermodynamic losses mapping.

The following assumptions are made in this work:

– The combined cycles operate in a steady-state mode.
– Pressure drops are assumed negligible.
– Changes in kinetic and potential energies are neglected.

From a second law point of view, it is important to quantify the exergy losses in each component in order to assess the overall performance of the system. Hence, mass, energy and exergy balance equations are applied to each component of the system described in Sect. 2.1. Neglecting kinetic and potential energies and exergy changes, these equations are:

$$\sum \dot{m}_{\mathrm{in}} - \sum \dot{m}_{\mathrm{out}} = 0 \tag{5}$$

$$\dot{Q}_{\mathrm{in}} + \dot{W}_{\mathrm{in}} + \sum_{\mathrm{in}} \dot{m}_{\mathrm{i}} h_{\mathrm{i}} = \dot{Q}_{\mathrm{out}} + \dot{W}_{\mathrm{out}} + \sum_{\mathrm{out}} \dot{m}_{\mathrm{i}} h_{\mathrm{i}} \tag{6}$$

$$\sum_{\mathrm{in}} \left(1 - \frac{T_0}{T_i}\right) \dot{Q}_i + \dot{W}_{in} + \sum_{in} \dot{m}_i ex_i = \sum_{out} \left(1 - \frac{T_0}{T_i}\right) \dot{Q}_i + \dot{W}_{out} + \sum_{out} \dot{m}_i ex_i + \dot{E}x_D \tag{7}$$

where $\dot{Q}$ is the rate of heat transfer between the control volume and its surroundings, $\dot{W}$ the rate of work, h the specific enthalpy and $\dot{E}x_D$ is the rate of exergy loss proportional to the entropy generated $\dot{S}_{gen}$ according to the Gouy-Stodola Theorem:

$$\dot{\mathrm{E}}\mathrm{x}_D = T_0 \dot{S}_{\mathrm{gen}} \tag{8}$$

with T_0 corresponding to the temperature of the surroundings.

The specific flow exergy, ex, is evaluated using the following expression:

$$\mathrm{ex} = \left(h - h_0\right) - T_0\left(s - s_0\right) \tag{9}$$

where the subscript *0* refers to the environment state.

The energy and exergy balances in Eqs. (6) and (7) were applied to each component of the system and the results obtained are summarized in Table 3.

The performance of the ORC systems is measured using the net power output and the total and individual exergy losses instead of thermal and exergy efficiency as the waste heat is free. The net power output of an ORC is defined as; $W_{\mathrm{net}} = W_{\mathrm{exp}} - W_{\mathrm{pump}}$. From an energy point of view, the performance of refrigeration systems is assessed by the coefficient of performance (*COP*), defined as the ratio of the cooling capacity to the power required to drive the compressor.

The overall coefficient of performance of the combined system, COP, can be determined as

$$\mathrm{COP} = \eta_{\mathrm{th}}\, \mathrm{COP}_{\mathrm{VCC}} \tag{10}$$

The components that affect the system performance are the compressor and the expander. The performance, security and reliability of the system depend on their designs. The compressor pressure ratio (CPR) and the expander volume ratio (EVR) are among the most important parameters that affect the design of these elements. They are defined as

$$\mathrm{CPR} = \frac{p_{11}}{p_{10}} \tag{11}$$

$$\mathrm{EVR} = \frac{v_4}{v_3} \tag{12}$$

Finally, the total mass flow rate of the working fluid for each kW refrigeration capacity is expressed as

$$\mathrm{MkW} = \frac{\dot{m}_{\mathrm{ORC}} + \dot{m}_{\mathrm{VCC}}}{\dot{Q}_{\mathrm{evap}}} \tag{13}$$

Table 3 Energy and exergy balances equations

Component	Energy balance	Exergy balance
ORC subsystem		
Basic ORC		
Expander	$\dot{W}_{\text{exp}} = \dot{m}_{\text{ORC}}\ (h_3\ -\ h_4)$	$\Delta\dot{E}x_{\text{exp}} = \dot{E}x_3 - \dot{E}x_4 - \dot{W}_{\text{exp}}$
Pump	$\dot{W}_p = \dot{m}_{\text{ORC}}\ (h_2\ -\ h_1)$	$\Delta\dot{E}x_p = \dot{E}x_1 - \dot{E}x_2 + \dot{W}_p$
Boiler	$\dot{Q}_{\text{b}} = \dot{m}_{\text{ORC}}\ (h_3 - h_2)$	$\Delta\dot{\text{E}}\text{x}_b = \dot{\text{E}}\text{x}_2\ -\ \dot{\text{E}}\text{x}_3\ +\ \dot{Q}_b\left(1 - \frac{T_0}{T_b^*}\right)$
Condenser	$\dot{Q}_{\text{cond}} = \dot{m}_{\text{ORC}}(h_4 - h_1)$	$\Delta\dot{\text{E}}\text{x}_{\text{cond}} = \dot{\text{E}}\text{x}_4\ -\ \dot{\text{E}}\text{x}_1$
Total system	$\eta_{\text{th}} = \left(\dot{W}_{\text{exp}}\ -\ \dot{W}_p\right)/\dot{Q}_{\text{b}}$	$\Delta\dot{E}_t = \sum_i \Delta\dot{E}_i$
Regenerative ORC		
Expander	$\dot{W}_{\text{exp}} = \dot{m}_{\text{ORC}}\ (h_3\ -\ h_4)$	$\Delta\dot{\text{E}}\text{x}_{\text{exp}} = \dot{E}x_3 - \dot{E}x_4 - \dot{W}_{\text{exp}}$
Pump	$\dot{W}_p = \dot{m}_{ORC}(h_2 - h_1)$	$\Delta\dot{E}x_p = \dot{E}x_1 - \dot{E}x_2 + \dot{W}_p$
Boiler	$\dot{Q}_b = \dot{m}_{ORC}(h_3 - h_5)$	$\Delta\dot{E}x_b = \dot{E}x_5 - \dot{E}x_3 + \dot{Q}_b\left(1 - \frac{T_0}{T_b^*}\right)$
Condenser	$\dot{Q}_{cond} = \dot{m}_{ORC}(h_6 - h_1)$	$\Delta\dot{\text{E}}\text{x}_{\text{cond}} = \dot{\text{E}}\text{x}_6 - \dot{\text{E}}\text{x}_1$
IHE	$\dot{Q}_{IHE} = \begin{cases} \dot{m}_{ORC}(h_4 - h_6) \\ \dot{m}_{ORC}(h_5 - h_2) \end{cases}$	$\Delta\dot{\text{E}}\text{x}_{\text{IHE}} = \dot{E}x_4 - \dot{E}x_6 + \dot{E}x_2 - \dot{E}x_5$
Total system	$\eta_{\text{th}} = \left(\dot{W}_{\text{exp}} - \dot{W}_p\right)/\dot{Q}_{\text{b}}$	$\Delta\dot{E}_t = \sum_i \Delta\dot{E}_i$
Serial Cascade ORC		
Expander	$\dot{W}_{\text{exp}} = \dot{m}_{ORC1}(h_3 - h_4) + \dot{m}_{ORC2}(h_{3'} - h_4)$	$\Delta\dot{E}x_{\text{exp}} = \dot{E}x_3 + \dot{E}x_{3'} - \dot{E}x_4 - \dot{W}_{\text{exp}}$
Pump 1	$\dot{W}_{p1} = \dot{m}_{ORC1}(h_2 - h_1)$	$\Delta\dot{E}x_{p1} = \dot{E}x_1 - \dot{E}x_2 + \dot{W}_{p1}$
Pump 2	$\dot{W}_{p2} = (\dot{m}_{ORC1} + \dot{m}_{ORC2})(h_6 - h_5)$	$\Delta\dot{E}x_{p2} = \dot{E}x_5 - \dot{E}x_6 + \dot{W}_{p2}$
Boiler 1	$\dot{Q}_{b1} = \dot{m}_{ORC1}(h_3 - h_2)$	$\Delta\dot{E}x_{b1} = \dot{E}x_2 - \dot{E}x_3 + \dot{Q}_{b1}\left(1 - \frac{T_0}{T_{b1}^*}\right)$
Boiler 2	$\dot{Q}_{b2} = \dot{m}_{ORC2}(h_{3'} - h_6) + \dot{m}_{ORC1}(h_1 - h_6)$	$\Delta\dot{E}x_{b2} = \dot{E}x_6 - \dot{E}x_{3'} - \dot{E}x_1 + \dot{Q}_{b2}\left(1 - \frac{T_0}{T_{b2}^*}\right)$
Condenser	$\dot{Q}_{cond} = (\dot{m}_{ORC1} + \dot{m}_{ORC2})(h_4 - h_5)$	$\Delta\dot{E}x_{cond} = \dot{E}x_4 - \dot{E}x_5$
Total system	$\eta_{th} = (\dot{w}_{\text{exp}} - \sum_i \dot{w}_{pi}) / \sum_i \dot{Q}_{bi}$	$\Delta\dot{E}_t = \sum_i \Delta\dot{E}_i$
VCC subsystem		
Evaporator	$\dot{Q}_{evap} = \dot{m}_{VCC}\left(h_{10} - h_{13}\right)$	$\Delta\dot{E}x_{evap} = \dot{E}x_{13} - \dot{E}x_{10} - \dot{Q}_{evap}\left(1 - \frac{T_0}{T_{evap}^*}\right)$
Compressor	$\dot{W}_{comp} = \dot{m}_{VCC}\left(h_{11} - h_{10}\right)$	$\Delta\dot{E}x_{comp} = \dot{E}x_{10} - \dot{E}x_{11} + \dot{W}_{comp}$
Condenser	$\dot{Q}_{cond} = \dot{m}_{VCC}\left(h_{11} - h_{12}\right)$	$\Delta\dot{E}x_{cond} = \dot{E}x_{11} - \dot{E}x_{12}$
Throttling valve	$h_{12} = h_{13}$	$\Delta\dot{E}x_v = \dot{E}x_{12} - \dot{E}x_{13}$
Total system	$\text{COP}_{\text{VCC}} = \dot{Q}_{\text{evap}}/\dot{W}_{\text{comp}}$	$\Delta\dot{E}_t = \sum_i \Delta\dot{E}_i$

3 Results and discussions

As stated previously, the aim of this study is to thermodynamically compare different ORC configurations in order to produce mechanical energy by recovering waste heat from a marine Diesel engine. This mechanical energy is used to drive a vapor compression refrigeration system. This section focuses on the comparison of the performance of ORC configuration using hydrocarbon-based working fluids, namely R600 and R600a. Three ORC configurations have been considered within the scope of this study: basic ORC cycle (ORC), organic Rankine cycle with internal heat exchanger (RORC) and cascaded organic Rankine cycle (SCORC).

Comparison has been carried out over evaporating temperature (t_{evap}) ranging from − 15 to 15 °C, boiling temperature (t_{b}) ranging from 60 to 90 °C which correspond to heat source temperature ranging from 70 to 100 °C, and condensing temperature (t_{cond}) ranging from 30 to 50 °C. The variation of these parameters has been carefully selected in order to remain within the typical operating conditions of ORC and VCC systems.

Generally, for higher heat sources temperatures, supercritical ORC cycles are more suitable for waste heat recovery

Table 4 Constant design and operating parameters for the analysis of the systems

Waste heat mass flow rate, kg/s	1.3
Heat source inlet temperature, °C	70–100 (80)
Boiling temperature, °C	60–90(70)
Evaporation temperature, °C	− 15 to 15 (5)
Condensation temperature, °C	30–50 (40)
Pump isentropic efficiency, %	75
Turbine isentropic efficiency, %	80
Compressor isentropic efficiency, %	75

Table 5 Verification case operating parameters

Working fluid mass flow rate in the ORC cycle	1 kg/s
Feed pump isentropic efficiency	75%
Boiler temperature	80 °C
Turbine isentropic efficiency	80%
Condenser temperature	40 °C
Evaporator temperature	5 °C
Isentropic efficiency of the compressor	75%

[41, 42]. The basic cycle has been used as reference for the other cycles. Therefore, its efficiency and power output are set to 100%. The analysis has been performed for several key operating parameters such as, the heat source temperature, the ORC condenser temperature and the VCC evaporator temperature. Table 4 summarizes constant design and operating parameters commonly used for ORC systems. Heat energy from engine cooling water is available at temperature ranging from 70 to 125 °C [14].

3.1 Model verification

The accuracy of simulation results is assessed by comparing the current results, using an in-house developed code, to the ones of the literature. The ORC efficiency, the VCC COP, the overall COP, the total mass flow rate of the working fluid for each kW refrigeration capacity (MkW), the compressor pressure ratio (CPR) and the expander volume ratio (*EVR*) are considered as the verification targets for a combine ORC-VCC system. Computations have been carried out according to the parameters listed in Table 5.

As can be clearly seen in Table 6, good agreements are observed between the results obtained from the code and those obtained from the literature. The relative error for all parameters remains below 5.4% justifying the reliability of the model proposed in predicting the performance of systems. In addition, the in-house code developed here offers the advantage of being more flexible in determining the cycle performance for different operating conditions.

3.2 ORC performances comparison

Figure 3 illustrates the effect of using IHE and cascade evaporation on the power produced on the shaft of the ORC expander. SCORC system produces additional power in comparison to the ORC and RORC systems. Therefore, splitting the evaporation process into two stages allows the system to produce more vapor which gives higher net power output. The output power produced by the ORC with internal heat exchanger is slightly higher than that produced by the simple ORC for a boiling temperature less than 79 °C.

The system net power output is the product of the enthalpy difference between the turbine inlet and outlet and the working fluid mass flow rate. For all refrigerants and configurations, the elevation of the heat source temperature raises the power output. Regardless of refrigerant used, the increase in heat source temperature results in a higher expansion pressure ratio, meaning that the enthalpy difference between the turbine inlet and outlet increases accordingly for all systems. However, for SCORC system, the mass flow rate of R134a decreases as the heat source temperature increases. Consequently, the combined effect of increasing the enthalpy difference and decreasing the mass flow rate of the working fluid will lead to a curve that has a maximum point of net power output.

From a thermodynamic point of view, refrigerants with higher critical temperatures can cover greater boiling

Table 6 Verification case results

Parameter	Present model			Li et al. [52]				Saleh [64]				Zheng et al. [70]	
	R134a	R600	R600a	R600	δ (%)	R600a	δ (%)	R600	δ (%)	R600a	δ (%)	R600a	δ (%)
η_{ORC} (%)	7.15	7.79	7.56	-	-	-	-	7.76	+0.39	7.57	− 0.13	-	-
COP_{VCC}	4.91	5.12	5.02	-	-	-	-	5.12	0	5.01	+0.2	-	-
COP_S	0.351	0.398	0.379	0.398	0	0.372	+1.88	0.398	0	0.380	− 0.26	0.383	− 1.04
MkW × 100	2.13	0.94	1.06	0.946	− 0.63	1.12	− 5.36	0.97	− 3.09	1.11	− 4.5	-	-
EVR	3.00	2.80	2.78	2.80	0	2.73	+1.83	2.81	− 0.36	2.75	+1.09	-	-
CPR	2.90	3.02	2.85	3.04	− 0.66	2.82	+1.06	3.04	− 0.66	2.85	0	-	-

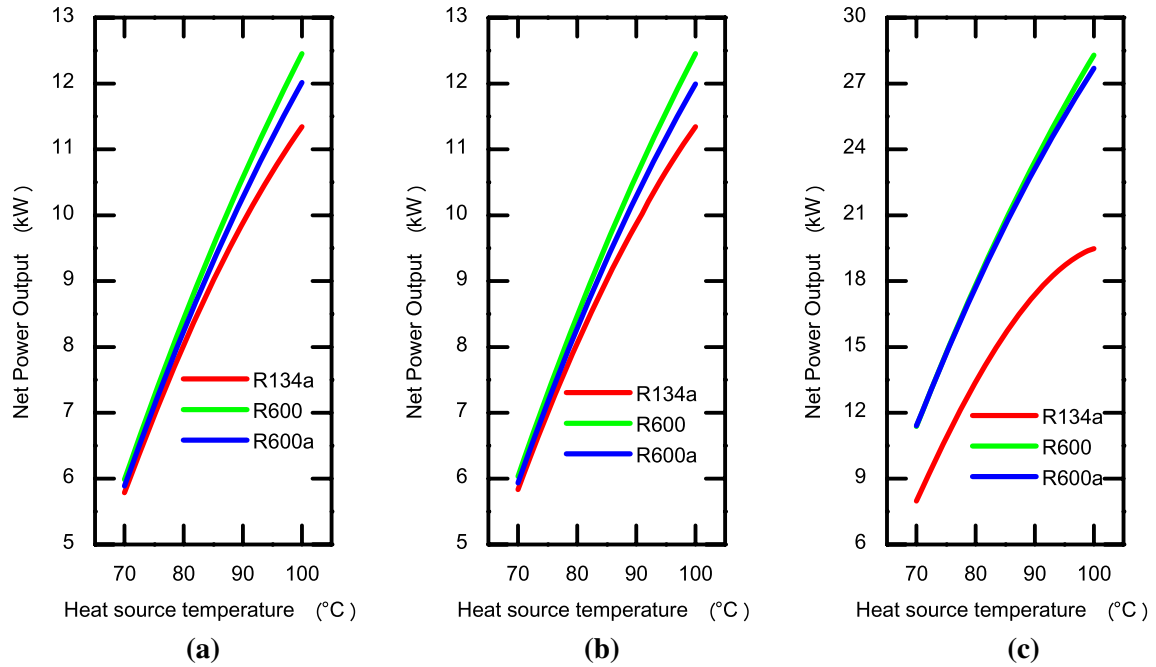

Fig. 3 Effect of the heat source temperature on the power produced on the ORC expander shaft: **a** ORC; **b** RORC; **c** SCORC ($T_{cond} = 40°C$, $\eta_{exp} = 80\%$, $\eta_p = 75\%$)

temperatures. Therefore they are particularly interesting for systems with high boiling temperatures. Thus as R600 has the highest critical temperature (425.15 K), it achieves the highest power output, followed in order by R600a (407.85 K) and R134a (374.25 K). It is also interesting to note that refrigerants with higher performances present lower operating pressures involving less design investment for the system.

The three system configurations have been also analyzed, from a second law point of view, by computing the total exergy loss. For each system, the total exergy loss is obtained from the sum of individual exergy losses of its components. Computations have been performed for an inlet heat source temperature of 80 °C, a condenser temperature of 40 °C and an expander isentropic efficiency of 80%. As illustrated in Fig. 4, it is clear that the cascade ORC produces the highest exergy loss rates (22.66–27.08 kW), followed in order by the simple ORC (12.75–13.15 kW) and the ORC with internal heat exchanger (12.73–13.12 kW).

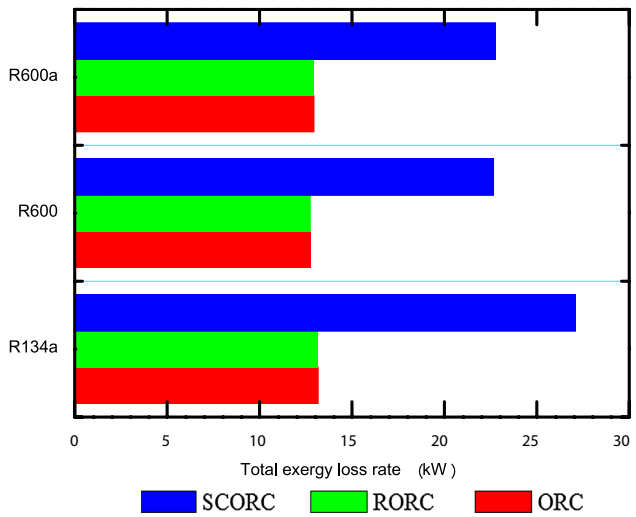

Fig. 4 Total exergy losses for different ORC configurations using various working fluids ($T_b = 70°C$, $T_{cond} = 40°C$, $\eta_{exp} = 80\%$, $\eta_p = 75\%$)

3.3 Combined ORC-VCC performances comparison

Figure 5 shows the effect of the heat source temperature on the COP and the MkW of the three systems studied for different working fluids. For all systems, the increase of the heat source temperature translates into an increase of the COP and a decrease in the MkW. The increase of the overall system COP is due to the fact that increasing the heat source temperature produces higher power on the expander shaft (increase of the thermal efficiency of the ORC subsystem), while the VCC COP remains constant. R600 performs the best followed, in order, by R600a and R134a. The difference between refrigerants is more pounced with the increase of the source temperature. Interestingly, the difference between the overall COP using different working fluids is lower for

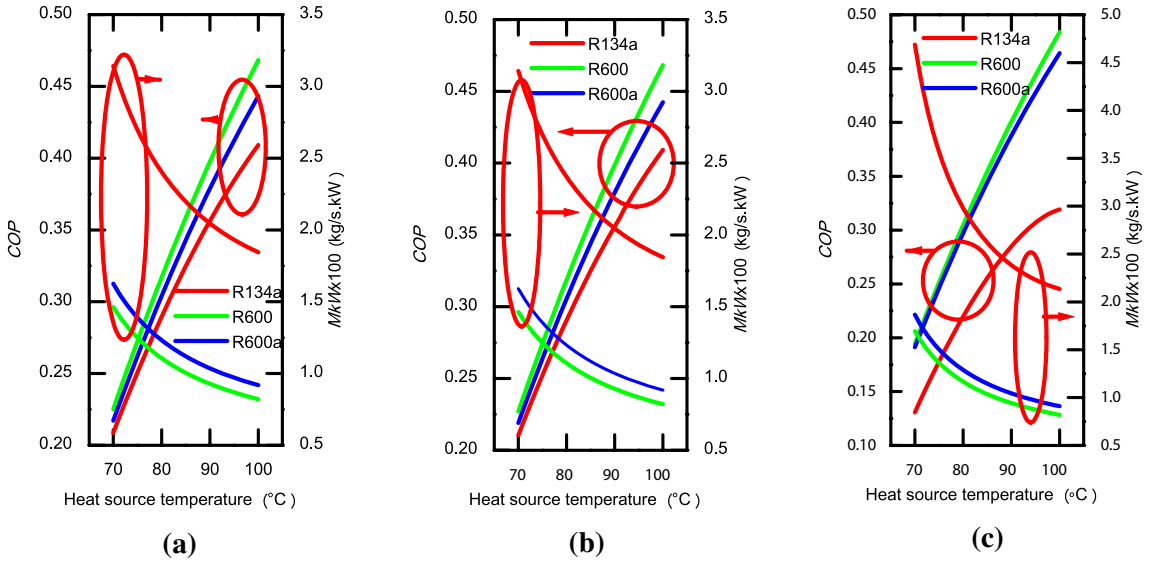

Fig. 5 Effect of the heat source temperature on the COP and MkW: **a** ORC-VCC; **b** RORC-VCC; **c** SCORC-VCC ($T_{cond} = 40°C$, $T_{evap} = 5°C$,$\eta_{exp} = 80\%$, $\eta_p = 75\%$, $\eta_{comp} = 75\%$)

reduced heat source temperatures. In addition to their thermodynamic performance, R600 and R600a operate under lower pressures compared to R134a. The maximum pressure for systems using these refrigerants does not exceed 1.83 MPa, resulting in lower system investments.

As it can be also observed in Fig. 6 that the MkW continues to decrease despite the fact that both the evaporator load (Q_{evap}) and the total mass flow rate increase with the rise of the heat source temperature. This trend can be explained by the fact that the evaporator load increases faster than the total mass flow rate as the heat source temperature increases. Both R600 and R600a return, by far, much lower MkW values compared to R134a. Furthermore, the SCORC configuration produces even lower

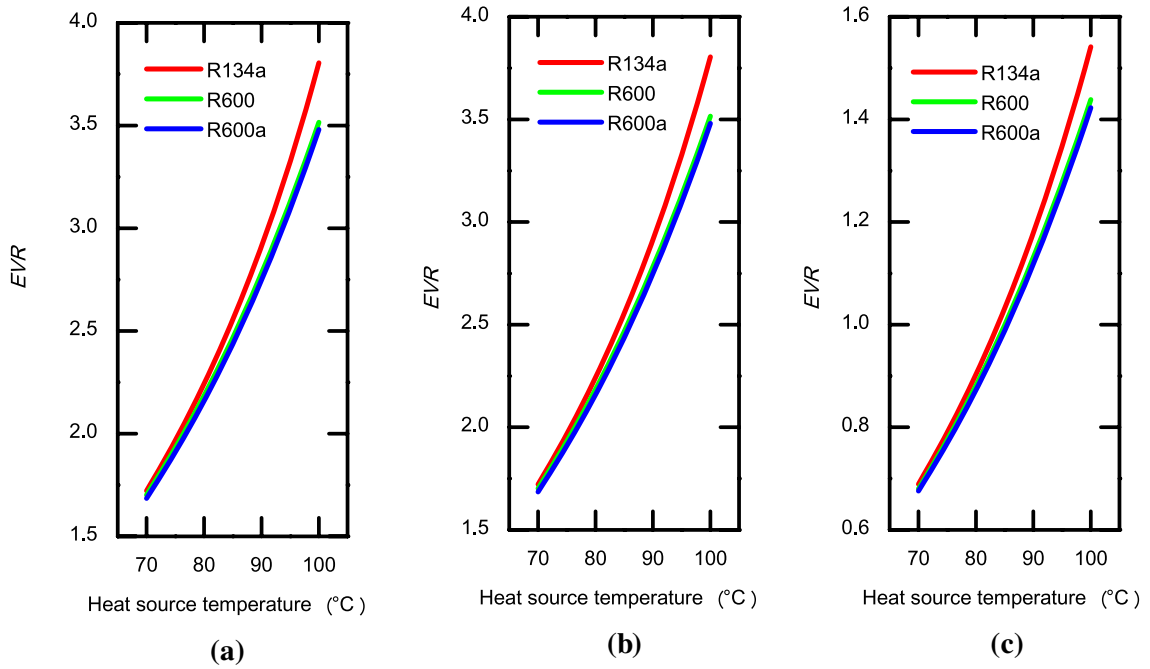

Fig. 6 Effect of the heat source temperature on the EVR: **a** ORC-VCC; **b** RORC-VCC; **c** SCORC-VCC ($T_{cond} = 40°C$, $T_{evap} = 5°C$,$\eta_{exp} = 80\%$, $\eta_p = 75\%$, $\eta_{comp} = 75\%$)

MkW values in comparison with the ORC and RORC configurations.

As depicted in Fig. 6, the expansion volume ratio, EVR, increases as the heat source temperature rises. This trend is due to the increase of the expander outlet specific volume and the decrease of the expander inlet specific volume pressure with the rise of the heat source temperature. Under the used operating conditions, the EVR values for all refrigerants remain smaller yielding to higher expander efficiency. It is also observed that the EVR values of the SCORC case are smaller, which means that the expander can be downsized.

Figure 7 indicates the variation of COP and MkW as function of the VCC evaporator temperature for the mentioned ORC subsystem configurations. For all cases, the COP increases while the MkW decreases when the VCC evaporator temperature is increased. The increase of the COP is mainly due to the increase of the VCC COP as the ORC thermal efficiency remains constant with the rise of the VCC evaporator temperature. On the other hand, the decrease of the MkW is attributed to the increase of the compressor inlet pressure as its outlet pressure remains unchanged. In this scenario, R600 performs the best followed, in order, by R600a and R134a in term of COP. Under the same operating conditions, the pressure difference between the compressor outlet and inlet using R134a as a refrigerant is much higher compared to R600 and R600a and consequently the compressor will consume much power reducing the performance of the system.

Figure 8 illustrates the variation of the CPR as a function of the evaporator temperature. For all refrigerants, the increase of the evaporator temperature causes a decrease of the CPR. Certainly, the rise of the evaporator temperature induces an increase of the compressor inlet pressure which reduces the power consumed by the compressor on one hand and increases the refrigeration effect on the other hand. It is interesting to note here that all system configurations produce comparable values of CPR.

The influence of the condenser temperature on the performance of the system is exhibited in Fig. 9. For all refrigerants, the overall COP is reduced as the condenser temperature increases. This is due to the conjugate effect of the condenser temperature on both the ORC and VCC subsystems. For the VCC subsystem, the increase of the condenser temperature induces an increase of the power consumed by the compressor and the diminution of the refrigeration effect, which results in a decrease of the VCC *COP*. Again, R600 produces the highest COP values followed, in order, by R600a and R134a.

An opposite trend is observed for the MkW. It increases with increasing the condenser temperature. This behavior is mainly attributed to the increase of the compressor outlet pressure as its inlet pressure remains unchanged with the rise of the condenser temperature.

The EVR decreases with increasing the condenser temperature (Fig. 10). It is clear that R600 and R600a present lower EVR values compared to R134a. However, the difference between EVR values among refrigerants is reduced for higher condenser temperature. On the other side, the CPR rises as the condenser temperature increases. This is mainly due to the increase of the compressor exit pressure as its inlet remains unchanged. This increase is more pounced for higher condenser temperatures.

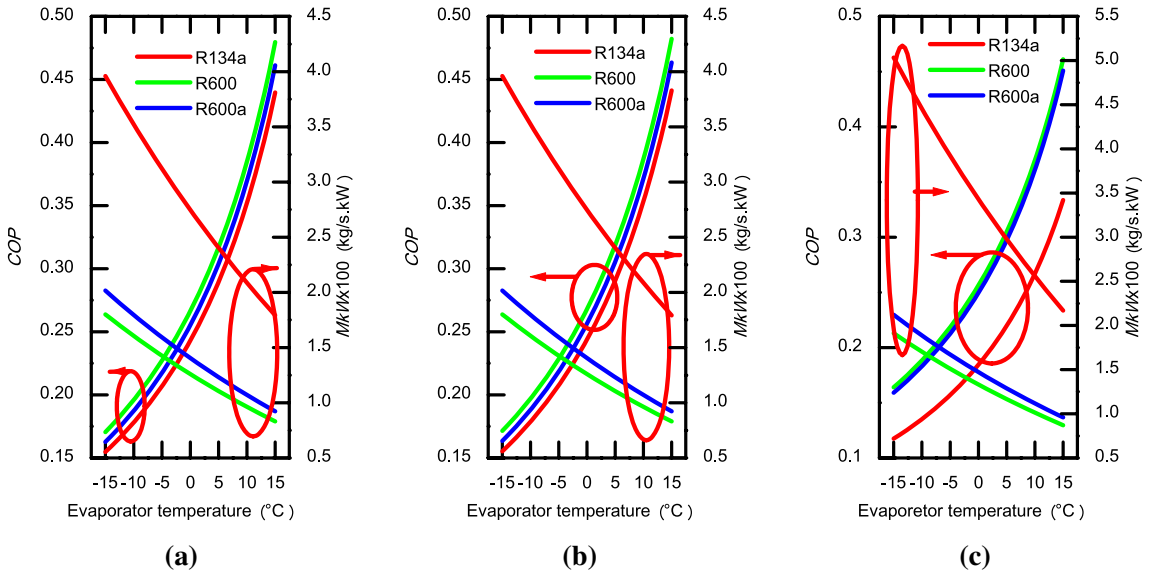

Fig. 7 Effect of the evaporator temperature on the *COP* and *MkW*: *a.* ORC-VCC; *b.* RORC-VCC; *c.* SCORC-VCC ($T_b = 70°C$, $T_{cond} = 40°C$, $\eta_{exp} = 80\%$, $\eta_p = 75\%$, $\eta_{comp} = 75\%$)

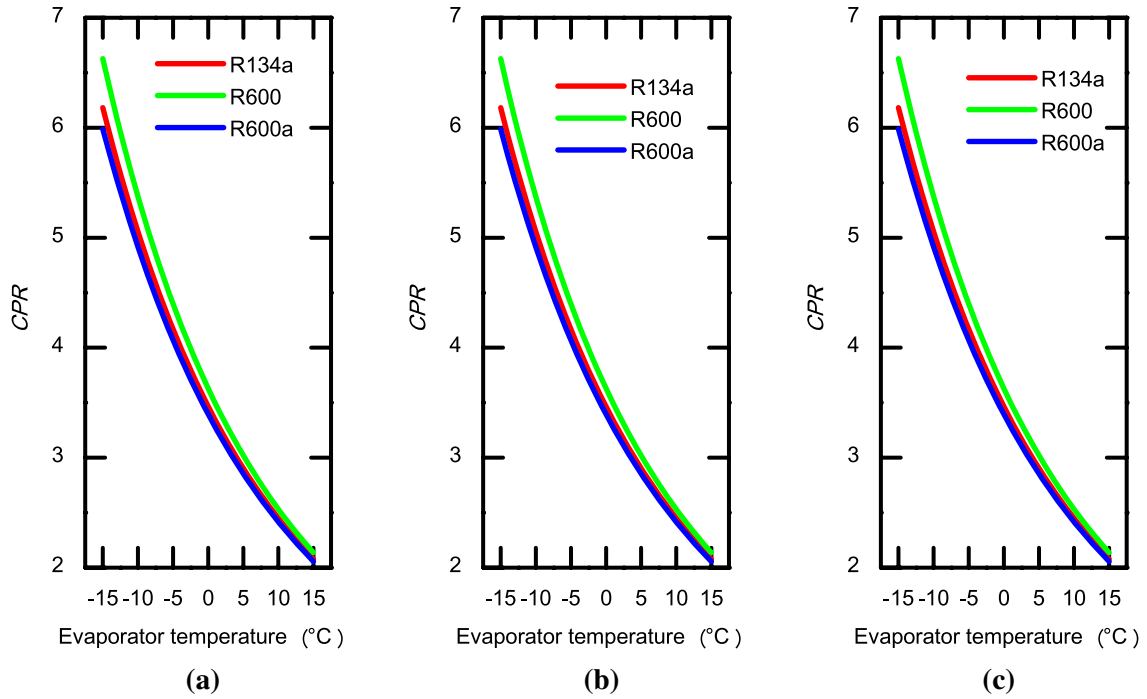

Fig. 8 Effect of the evaporator temperature on the *CPR*: *a.* ORC-VCC; *b.* RORC-VCC; *c.* SCORC-VCC ($T_b = 70°C$, $T_{cond} = 40°C$, $\eta_{exp} = 80\%$, $\eta_p = 75\%$, $\eta_{comp} = 75\%$)

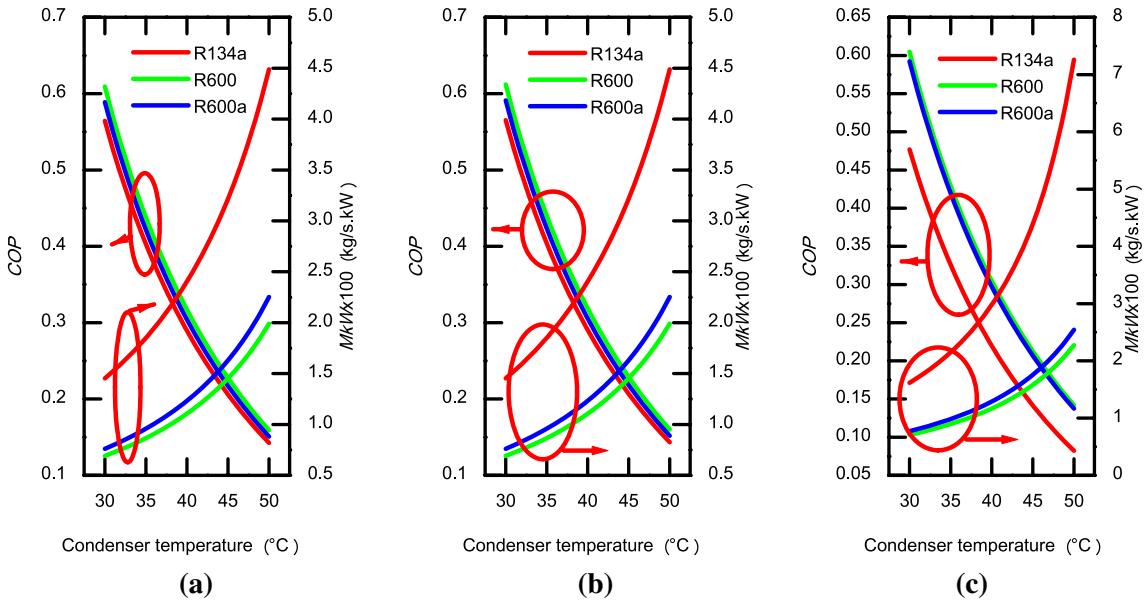

Fig. 9 Effect of the condenser temperature on the *COP* and *MkW*: **a** ORC-VCC; **b** RORC-VCC; **c** SCORC-VCC ($T_b = 70°C$, $T_{evap} = 5°C$, $\eta_{exp} = 80\%$, $\eta_p = 75\%$, $\eta_{comp} = 75\%$)

In order to examine the overall performance of the system, the exergy destruction in each component of the system is evaluated and related to the total exergy destruction in the system. The rate of exergy destruction for the *k*th component can be compared to the exergy input rate using by:

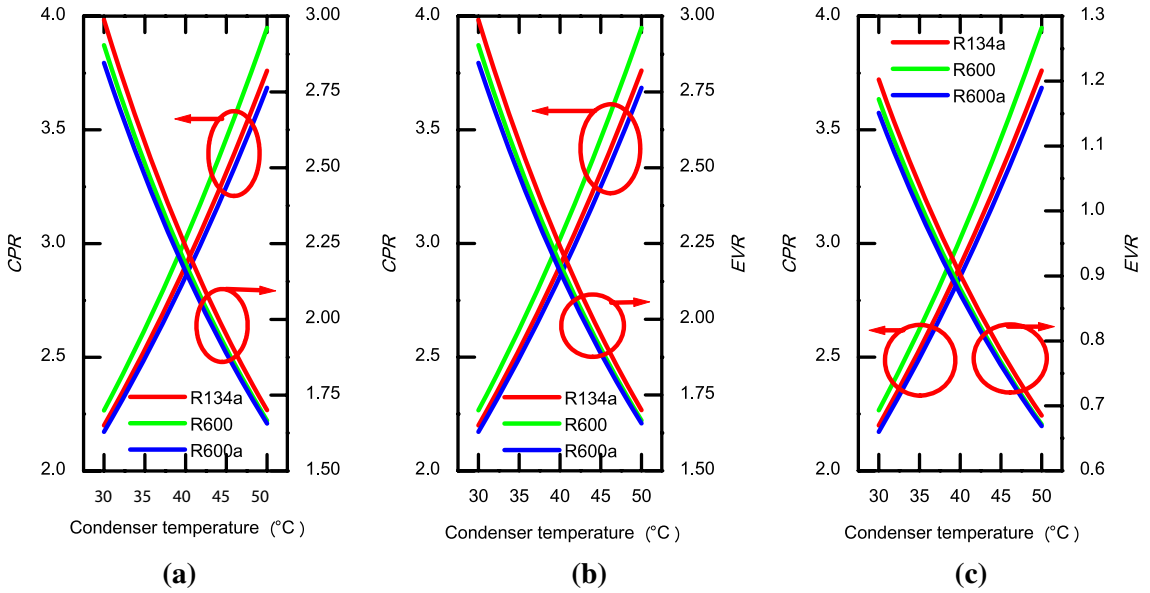

Fig. 10 Effect of the condenser temperature on the *CPR* and *EVR*: *a.* ORC-VCC; *b.* RORC-VCC; *c.* SCORC-VCC ($T_b = 70°C$, $T_{evap} = 5°C$, $\eta_{exp} = 80\%$, $\eta_p = 75\%$, $\eta_{comp} = 75\%$)

$$\%\Delta\dot{E}x_k = \frac{\Delta\dot{E}x_k}{\dot{E}x_t} \times 100 \tag{14}$$

Computations have been performed for an inlet heat source temperature of 80 °C, a condenser temperature of 40 °C, an expander isentropic efficiency of 80% and a compressor isentropic efficiency of 75%.

As shown in Fig. 11, the maximum exergy loss belongs to the heat ORC condenser followed, in order, by the VCC evaporator, the ORC boiler, the VCC condenser, the VCC compressor, the ORC expander, the VCC throttling valve and the ORC pump. Thus, based on this exergy analysis, efforts should be focused on the improvement of components presenting higher exergy losses such as the four heat exchangers, the expander and the compressor. The exergy loss in the heat exchangers is exclusively due to the heat transfer from one stream to another, while exergy losses in the expander and the compressor mainly originate from the fluid dissipation and friction. Results indicate also that butane performs the best due to its lower total exergy loss. The results also show that using serial cascade evaporation instead of single evaporation causes a reduction in exergy losses in the expander. The incorporation of an IHE reduces exergy losses in the ORC boiler and the ORC condenser. As expected, total exergy losses in the RORC-VCC (23.1–23.69 kW) and SCORC-VCC (44.32–44.64 kW) systems are greater than the total exergy loss of the ORC-VCC system (23.09–23.68 kW) due mainly to supplementary components included in those systems and the rise of working fluid mass flow rate in the VCC system.

Finally, in most previous studies on ORC-VCC systems, the same working fluid is generally used for both the ORC and VCC subsystems. The purpose of this section is to show the effect of using different refrigerants in the ORC and VCC subsystems on the performance of the combined ORC-VCC system. It is more interesting to choose a dry fluid among the refrigerant studied as a working fluid in the ORC subsystem, while varying the refrigerant in the VCC subsystem.

Table 7 summarizes results of varying refrigerants in the ORC and VCC subsystems. As can be observed in the table, the combined system performance is the highest when using R600 and R600a in the ORC and VCC subsystems, respectively.

4 Conclusions

In this paper, various configurations of ORC systems have been studied and compared using both the first and second laws of thermodynamics. Eco-friendly refrigerants, namely butane (R600) and isobutane (R600a) have been used as working fluids. Carrying out a thermodynamic analysis is actually requirement in order to optimize the performance of a given ORC-VCC configuration before building the system test bed for experiments. Undoubtedly, a real system is more complicated than the system analyzed in the present study, but the main conclusions drawn from the actual simple theoretical system should remain valid.

The thermodynamic model presented has been implemented in an in-house code written in Fortran. This code has been validated by comparing its results with those obtained

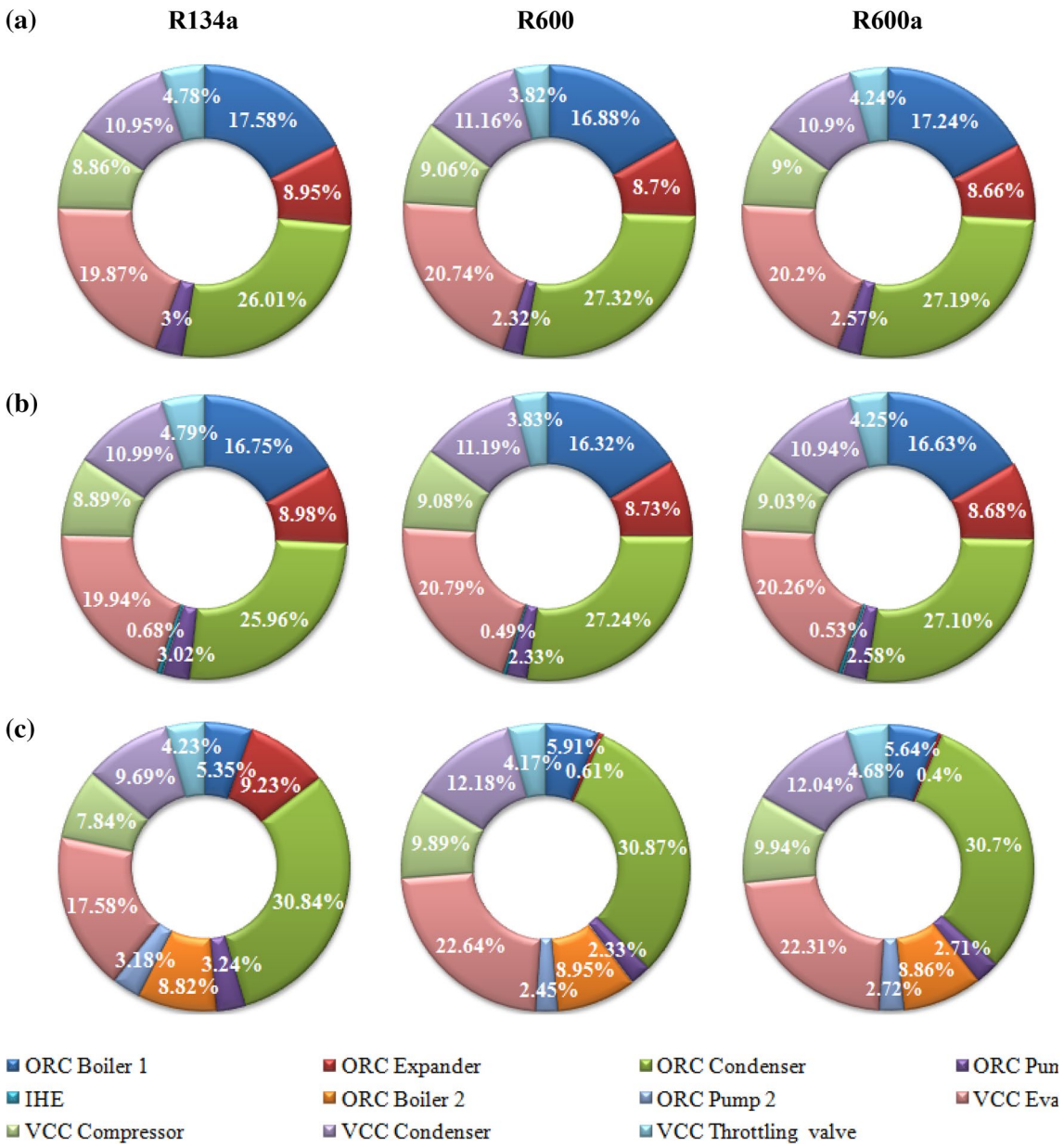

Fig. 11 Components exergy losses for various working fluids: **a** ORC-VCC; **b** RORC-VCC; **c** SCORC-VCC ($T_b = 70°C$, $T_{cond} = 40°C$, $T_{evap} = 5°C$, $\eta_{exp} = 80\%$, $\eta_p = 75\%$, $\eta_{comp} = 75\%$)

using the more established *Solkane* software. The comparison among the obtained results confirms the reliability of the presented model. Furthermore, the developed code can be modified or updated easily with the possibility to be linked to design and optimization subroutines in order to simulate real systems.

The main conclusions to be drawn from the present study may be summarized as follows:

- The RORC and SCORC exhibit, respectively, an average of 0.52% and 2.41% higher COP values than the simple ORC under considered conditions.
- The overall system performance improvement is more affected by the boiler temperature than the evaporator temperature.
- The addition of an internal heat exchanger do not necessary improves the overall COP or the net power output. This finding is actually in agreement with some studies reported in the open literature (see for example [43]) nevertheless the improvement the overall COP with a decrease in the net power output is also reported (see for example [44]).
- The present exergy analysis has allowed a mapping of exergy losses in the system. Based on this, it is suggested

Table 7 Effect of the nature of the working fluid in ORC and VCC subsystems on the overall of the combined system

ORC working fluid	VCC working fluid	η_{ORC} %	COPVCC	COP
	R134a	5.904	4.901	0.289
R134a	R600	5.904	5.116	0.302
	R600a	5.904	5.017	0.296
	R134a	6.198	4.901	0.304
R600	R600	6.198	5.116	0.317
	R600a	6.198	5.017	0.311
	R134a	6.061	4.901	0.297
R600a	R600	6.061	5.116	0.310
	R600a	6.061	5.017	0.304

that future efforts should be focused on components with higher exergy losses in order to further improve the overall performance of the system.

– Finally, it has been revealed that R600 performs the best if it is used in both the ORC and VCC subsystems.

For future work, the authors are intending to build an experimental rig in order to further confirm the present findings and address the system optimization objectives outlined in the present study.

References

1. D. Barki, J. Rogers, United Nations conference on trade and development (UNCTAD), New York and Geneva. Review of maritime transport, 2015, pp. 1–122.
2. Tse LKC., Wilkins S., McGlashan N., Urban B., Martinez-Botas R. Solid oxide fuel cell/gas turbine trigeneration system for marine applications. J. Power Sources 196, 3149–3162 (2011).
3. E. Tzannatos, Ship emissions and their externalities for Greece. Atmos Environ **44**, 2194–2202 (2010)
4. N. Heitmann, S. Khalilian, Accounting for CO_2 emissions from international shipping: Burden sharing under different UNFCCC allocation options and regime scenarios. Kiel Working Paper No. 1665, October 2010.
5. V. Eyring, H.W. Kohler, J. van Aardenne, Lauer A (2005) Emissions from international shipping: 1. The last 50 years. J. Geophys. Res. **110**, 17305 (2005)
6. S. Alvik, M.S. Eide, Ø. Endresen, P. Hoffmann, T. Longva, Pathways to low carbon shipping: Abatement potential towards 2030. DNV, Norway, 2009
7. G. Bidini, F. Di Maria, M. Generosi, Micro-cogeneration system for a small passenger vessel operating in a nature reserve. Appl. Therm. Eng. **25**, 851–865 (2005)
8. R. Balaji, O. Yaakob, K.K. Koh, F.A. Adnan, N. Ismail, B. Ahmad, M.A. Ismail, Y.R. Vern, Comparison of heat exchanger designs for ship ballast water heat treatment system. J. Teknologi. (2015). https://doi.org/10.11113/jt.v77.6149
9. P. Marty, Ship energy efficiency study: development and application of an analysis method, PhD Thesis. Ecole Centrale de Nantes, France, 2014.
10. A. Ouadha, Y. El Gotni, Integration of an ammonia-water absorption refrigeration system with a marine diesel engine: a thermodynamic study. Procedia Comput. Sci. **19**, 754–761 (2013)
11. U. Larsen, O. Sigthorsson, F. Haglind, A comparison of advanced heat recovery power cycles in a combined cycle for large ships. Energy **74**, 260–268 (2014)
12. B.F. Tchanche, G. Lambrinos, A. Frangoudakis, G. Papadakis, Low-grade heat conversion into power using organic Rankine cycles-a review of various applications. Renew. Sustain. Energy Rev. **15**, 3963–3979 (2011)
13. Z. Shengjun, W. Huaixin, G. Tao, Performance comparison and parametric optimization of subcritical Organic Rankine Cycle (ORC) and transcritical power cycle system for low-temperature geothermal power generation. Appl. Energy **88**, 2740–2754 (2011)
14. G. Shu, Y. Liang, H. Wei, H. Tian, J. Zhao, L. Liu, A review of waste heat recovery on two-stroke IC engine abroad ships. Renew. Sustain. Energy Rev. **19**, 385–401 (2013)
15. U. Larsen, L. Pierobon, F. Haglind, C. Gabrielli, Design and optimisation of organic Rankine cycles for waste heat recovery in marine applications using the principles of natural selection. Energy **55**, 803–812 (2013)
16. M.H. Yang, R.H. Yeh, Analyzing the optimization of an organic Rankine cycle system for recovering waste heat from a large marine engine containing a cooling water system. Energy Convers. Manag. **88**, 999–1010 (2014)
17. W. Schwarz, J.M. Rhiemeier, The analysis of the emissions of fluorinated greenhouse gases from refrigeration and air conditioning equipment used in the transport sector other than road transport and options for reducing these emissions. Maritime, Rail, and Aircraft Sector e final report. European Commission, 2 November 2007.
18. X. Xu, Y. Li, S.Y. Yang, G. Chen, A review of fishing vessel refrigeration systems driven by exhaust heat from engines. Appl. Energy **203**, 657–676 (2017)
19. D. Prigmore, R. Barber, Cooling with the Sun's heat design consideration and test data for a Rankine cycle prototype. Sol. Energy **17**, 185–192 (1975)
20. N. Lior, Solar energy and the steam Rankine cycle for driving and assisting heat pumps in heating and cooling modes. Energy Convers. **16**, 111–123 (1977)
21. E. Wali, Optimum working fluids for solar powered Rankine cycle cooling of buildings. Sol. Energy **25**, 235–241 (1980)
22. F.R. Biancardi, J.W. Sitler, G. Melikian, Development and test of solar Rankine cycle heating and cooling system. Int. J. Refrig. **5**, 351–360 (1982)
23. M.O. Nazer, S.M. Zubair, Analysis of Rankine cycle air-conditioning systems. ASHRAE J. **88**, 332–334 (1982)
24. K. Koai, N. Lior, H. Yeh, Performance analysis of a solar powered/fuel-assisted Rankine cycle with a novel 30 hp turbine. Sol. Energy **32**, 753–764 (1984)
25. A.N. Eğrican, A. Karakas, Second law analysis of a solar powered Rankine cycle/vapor compression cycle. J. Heat Recovery Syst. **6**, 135–141 (1986)
26. S. Christensen, An evaluation of a rankine cycle driven heat pump. Heat Recovery Syst. CHP **10**, 161–175 (1990)
27. O. Bounefour, A. Ouadha, Thermodynamic analysis and thermodynamic analysis and working fluid optimiazation of a combined ORC-VCC system using waste heat from a marine diesel engine. Proceedings of the ASME 2014 International Mechanical Engineering Congress and Exposition IMECE2014, Montreal, Quebec, Canada.
28. M.A. Hammad, M.A. Alsaad, The use of hydrocarbon mixtures as refrigerants in domestic refrigerator. Appl. Thermal Eng. **19**, 1181–1189 (1999)

29. D. Jung, C.B. Kim, K. Song, B. Park, Testing of propane/isobutane mixture in domestic refrigerators. Int. J. Refrig. **23**, 517–527 (2000)
30. B. Jacob, A. Azar, P. Neksa, Performance of CO_2-refrigeration (R-744) in commercial cold drink equipment. In 7th IIR Gustav Lorentzen Conference on Natural Working Fluids, May 28–31, 2006.
31. C. Rohrer, Transcritical CO_2 bottle cooler development. In 7th IIR Gustav Lorentzen Conference on Natural Working Fluids, May 28–31, 2006.
32. M. Mohanraj, S. Jayaraj, C. Muraleedharan, P. Chandrasekar, Experimental investigation of R290/R600a mixture as an alternative to R134a in a domestic refrigerator. Int. J. Thermal Sci. **48**, 1036–1042 (2009)
33. L. Cecchinato, M. Corradi, Transcritical carbon dioxide small commercial cooling applications analysis. Int. J. Refrig. **34**, 50–62 (2011)
34. E. Da Riva, D. Del Col, Performance of a semi-hermetic reciprocating compressor with propane and mineral oil. Int. J. Refrig. **34**, 752–763 (2011)
35. M. Rasti, F.A. Seyed, M. Hatamipour, Energy efficiency enhancement of a domestic refrigerator using R436a and R600a as alternative refrigerants to R134a. Int. J. Therm. Sci. **74**, 86–94 (2013)
36. M.G. He, X.Z. Song, H. Liu, Y. Zhang, Application of natural refrigerant propane and propane/isobutane in large capacity chest freezer. Appl. Therm. Eng. **70**, 732–736 (2014)
37. S. Elbel, Y.P. Fuentes, C. Bowers, P. Hrnjak, Successful conversion and validation of glass door merchandisers using transcritical R744. in 11th IIR Gustav Lorentzen Conference on Natural Refrigerants, August 31–September 2, 2014.
38. C.C. Yu, T.P. Teng, Retrofit assessment of refrigerator using hydrocarbon refrigerants. Appl. Therm. Eng. **66**, 507–518 (2014)
39. ANSI/ASHRAE Addenda Supplement. Designation and Safety Classification of Refrigerants, ISSN: 1041-2336 (2015).
40. J.M. Calm, G.C. Hourahan, Refrigerant data update. Hpac Eng. **79**, 50–64 (2007)
41. A.B. Little, S. Garimella, Comparative assessment of alternative cycles for waste heat recovery and upgrade. Energy **36**, 4492–4504 (2011)
42. H. Gao, C. Liu, C. He, X. Xu, S. Wu, Y. Li, Performance analysis and working fluid selection of a supercritical organic Rankine cycle for low grade waste heat recovery. Energies **5**, 3233–3247 (2012)
43. Y. Dai, J. Wang, L. Gao, Prametric optimization and comparative study of organic Rankine cycle (ORC) for low grade waste heat recovery. Energy Convers. Manag. **50**, 576–582 (2009)
44. W. Li, X. Feng, L.J. Yu, J. Xu, Effects of evaporating temperature and internal heat exchanger on organic Rankine cycle. Appl. Therm. Eng. **31**, 4014–4023 (2001)
45. S.C. Kaushik, M. Singh, A. Dubey, Thermodynamic modelling of single/dual organic fluid Rankine cycle cooling systems: a comparative study. Int J Ambient Energy **15**(1), 37–50 (1994)
46. J. Jeong, Y.T. Kang, Analysis of a refrigeration cycle driven by refrigerant steam turbine. Int. J. Refrig. **27**, 33–41 (2004)
47. S. Aphornratana, T. Sriveerakal, Analysis of a combined Rankine-vapor-compression refrigeration cycle. Energy Convers. Manage. **51**, 2557–2564 (2010)
48. H. Wang, R. Peterson, K. Harada, E. Miller, R. Ingram-Goble, L. Fisher, J. Yih, C. Ward, Performance of a combined organic Rankine cycle and vapor compression cycle for heat activated cooling. Energy **36**, 447–458 (2011)
49. H. Wang, R. Peterson, T. Herron, Design study of configurations on system COP for a combined ORC (organic Rankine cycle) and VCC (vapor compression cycle). Energy **36**, 4089–4820 (2011)
50. M. Aneke, B. Agnew, C. Underwood, M. Menkiti, Thermodynamic analysis of alternative refrigeration cycles driven from waste heat in a food processing application. Int. J. Refrig. **35**, 1349–1358 (2012)
51. J. Demierre, S. Henchoz, D. Favrat, Prototype of a thermally driven heat pump based on integrated Organic Rankine Cycle (ORC). Energy **41**, 10–17 (2012)
52. H. Li, X. Bu, L. Wang, Z. Long, Y. Lian, Hydrocarbon working fluids for a Rankine cycle powered vapor compression refrigeration system using low grade thermal energy. Energy Build. **65**, 167–172 (2013)
53. X. Bu, L. Wang, H. Li, Performance analysis and working fluid selection for geothermal energy-powered organic Rankine-vapor compression air conditioning. Geotherm. Energy **1**, 1–14 (2013)
54. X.B. Bu, H.S. Li, L.B. Wang, Performance analysis and working fluids selection of solar powered organic Rankine-vapor compression ice maker. Sol. Energy **95**, 271–278 (2013)
55. X. Bu, L. Wang, H. Li, Working fluids selection for fishing boats waste heat powered organic Rankine-vapor compression ice maker. Heat Mass Transf. **50**, 1479–1485 (2014)
56. J. Demierre, D. Favrat, J. Schiffmann, J. Wegele, Experimental investigation of a thermally driven heat pump based on a double organic rankine cycle and an oil-free compressor-turbine unit. Int. J. Refrig. **44**, 91–100 (2014)
57. Y.R. Li, X.Q. Wang, X.P. Li, J.N. Wang, Performance analysis of a novel power/refrigerating combined-system driven by the low-grade waste heat using different refrigerants. Energy **73**, 543–553 (2014)
58. Yilmaz, Transcritical organic Rankine vapor compression refrigeration system for intercity bus air-conditioning using engine exhaust heat. Energy 82, 1047–1056 (2015).
59. F. Molés, J.N. Esbrí, B. Peris, A.M. Babiloni, K. Kontomaris, Thermodynamic analysis of a combined organic Rankine cycle and vapor compression cycle system activated with low temperature heat sources using low GWP fluids. Appl. Therm. Eng. **87**, 444–453 (2015)
60. K.H. Kim, H.P. Blanco, Performance analysis of a combined organic Rankine cycle and vapor compression cycle for power and refrigeration cogeneration. Appl. Therm. Eng. **91**, 964–974 (2015)
61. C. Yue, F. You, Y. Huang, Thermal and economic analysis of an energy system of an ORC coupled with vehicle air conditioning. Int. J. Refrig. **64**, 152–167 (2016)
62. M.T. Nasir, K.C. Kim, Working fluids selection and parametric optimization of an Organic Rankine Cycle coupled Vapor Compression Cycle (ORC-VCC) for air conditioning using low grade heat. Energy Build. **129**, 378–395 (2016)
63. S. Karellas, K. Braimakis, Energy–exergy analysis and economic investigation of a cogeneration and trigeneration ORC–VCC hybrid system utilizing biomass fuel and solar power. Energy Convers. Manag. **107**, 103–113 (2016)
64. B. Saleh, Parametric and working fluid analysis of a combined organic Rankine-vapor compression refrigeration system activated by low-grade thermal energy. J. Adv. Res. **7**(5), 651–660 (2016)
65. Lizarte R., Palacios-Lorenzo, Marcos J.D., Parametric study of a novel organic Rankine cycle combined with a cascade refrigeration cycle (ORC-CRS) using natural refrigerants. Appl. Thermal Eng. 127, 378–389 (2017).
66. D. Wu, L. Aye, T. Ngo, P. Mendis, Optimisation and financial analysis of an organic Rankine cycle cooling system driven by facade integrated solar collectors. Appl. Energy **185**, 172–182 (2017)
67. K. Braimakis, A. Thimo, S. Karellas, Technoeconomic analysis and comparison of a solar-based biomass ORC-VCC system and a PV heat pump for domestic trigeneration. J. Energy Eng. **143**(2), 04016048 (2017)

68. O. Bounefour, A. Ouadha, Performance improvement of combined organic Rankine-vapor compression cycle using serial evaporation in the organic cycle. Energy Procedia **139**, 248–253 (2017)
69. B. Saleh, Energy and exergy analysis of an integrated organic Rankine cycle-vapor compression refrigeration system. Appl. Thermal Eng. **141**, 697–710 (2018)
70. N. Zheng, J. Wei, L. Zhao, Analysis of a solar Rankine cycle powered refrigerator with zeotropic mixtures. Sol. Energy **162**, 57–66 (2018)
71. N. Javanshir, S.M.S. Mahmoudi, M.A. Rosen, Thermodynamic and exergoeconomic analyses of a novel combined cycle comprised of vapor-compression refrigeration and organic rankine cycles. Sustainability **11**, 1–20 (2019)
72. B. Saleh, Ayman A. Aly, Ageel F. Alogla, Awad M. Aljuaid, Mosleh M. Alharthi, Khaled I.E. Ahmed, Y.S. Hamed, Performance investigation of organic Rankine-vapor compression refrigeration integrated system activated by renewable energy. Mech. Ind. 20, 206 (2019).
73. M.T. Nasir, M.A. Ali, T.S. Khan, E. Al-Hairi, M.B. Kadri, K.C. Kim, Performance assessment and multi objective optimization of an Organic Rankine Cycle driven cooling air conditioning system. Energy Build. **191**, 13–30 (2019)
74. Y. Liang, Z. Yu, W. Li, A waste heat-driven cooling system based on combined organic rankine and vapour compression refrigeration cycles. Appl. Sci. **9**, 4242 (2019)